Silicon (2023) 15:5271–5281
https://doi.org/10.1007/s12633-023-02428-0

RESEARCH

Fabrication, Microstructural, and Mechanical Behavior of SiC Composite with Insitu Formation of BN and Si_3N_4

Aman Singh[1] · Vinay Kumar Singh[1] · Raj Kumar Chaturvedi[1] · Jyoti Kumari[1] · N. K. Debnath[1]

Received: 8 January 2023 / Accepted: 21 March 2023 / Published online: 31 March 2023

Abstract
Dealing with high-temperature properties and brittleness and is always one of the hot topics in the field of ceramic materials. Extensive research has been carried out for it and Si_3N_4-SiC composites are one of the most promising composites. In this study, the impact of Si_3N_4 and BN reinforcement on the microstructure and physio-mechanical properties of SiC-based composites were explored. Two sets of composites, including Si_3N_4-SiC and BN-Si_3N_4-SiC aided with Al_2O_3, were fabricated using nitridation of Si and B_2O_3 at 1450 °C. The mechanical properties, microstructure, phase transformation, densification, and porosity were depicted and discussed. X-ray diffraction patterns revealed the insitu formation of Si_3N_4 (both α and β phases) and BN in the final composite. The specimen with 10% Si and 10% B_2O_3 possessed the superior flexural strength (284.4 MPa) with excellent hardness (23.4 GPa). The incorporation of BN is found to enhance the mechanical properties especially hardness while overcoming the shortcomings of reaction-bonded Si_3N_4-SiC. The corresponding densification and strengthening mechanism were explained in this paper.

Keywords Si_3N_4-SiC refractories · Boron nitride · Mechanical properties · Flexural strength

1 Introduction

Technological developments in aerospace, marine, nuclear, and refractory industries, among others, increase the demand for more robust materials [1–3]. Ceramics composites can meet such applications in harsh environments, but further advancements are necessary [4, 5].

Silicon carbide (SiC) and Silicon nitride (Si_3N_4) are known for their excellent thermal and mechanical properties. SiC exhibit strong wear, creep, and oxidation resistance at higher temperatures but has a lesser fracture toughness [6]. Si_3N_4 ceramics, on the other hand, have more substantial flexural strength and fracture toughness but weaker oxidation resistance at extreme temperatures [7, 8]. Si_3N_4–SiC composite prepared using Si_3N_4 powders has been widely reported with complex and expensive sintering processes such as SPS [8], Hot-pressed sintering at 1850 °C [9], sintering-post-HIP at around 2000 °C [10]. On the other hand, using Si powders instead of Si_3N_4 for synthesizing Si_3N_4–SiC composites can have economic benefits due to the low cost of the Silicon powder. Thus, the nitridation of silicon in controlled environment furnaces is a suitable method for producing reaction bonded silicon nitride-silicon carbide composites. Direct nitridation of Si powder at 1414 °C (Melting point of Si) could produce a reaction bonded Si_3N_4–SiC composite. Additionally, reports suggest SiC-Si_3N_4 reaction bonded composites fabricated at 1450 °C via pressure-less sintering have better densification with improved overall properties [11, 12].

The sintering of Si_3N_4-SiC composite is challenging without any additives due to Si's high covalence and low diffusivity [13]. Also, an effective method for further enhancing the high-temperature properties is by promoting the amorphous phase crystallization and increasing the refractoriness of the grain boundary phase [14]. This could be achieved by adding appropriate sintering aids in the composite. MgO, AlN, Y_2O_3, Al_2O_3, and oxides of some rare earth have been reported as a sintering aid in the hybrid composite system [15–19]. Al_2O_3 has been known as the most cost-effective in comparison with rest while improving oxidation resistance and reducing linear shrinkage. Al_2O_3 forms a glassy phase on interacting with SiO_2 formed during the oxidization of

✉ Vinay Kumar Singh
vinaycer@gmail.com

[1] Department of Ceramic Engineering, Indian Institute of Technology (BHU) Varanasi, Varanasi, India 221005

Si_3N_4 and SiC, which shields against further oxidation and corrosion [20–23].

Reaction-bonded Si_3N_4 tends to have a porous structure which degrades its mechanical properties and oxidation resistance. To overcome this, B_2O_3 can be added to the composite, whose nitridation forms boron nitride (BN). BN has excellent hardness, thermal shock resistance, and machinability, which would overcome the shortcomings of Si_3N_4-SiC composites [24–26].

The development of SiC composites with in-situ formation of BN and Si_3N_4 is a novel and important topic in the field of advanced ceramics. SiC is a well-known engineering material with excellent mechanical and thermal properties, but its brittle nature limits its application in certain areas. The addition of BN and Si_3N_4 can enhance the fracture toughness and thermal shock resistance of SiC composites, thereby extending their range of applications. In-situ formation of these phases during the processing of SiC composites eliminates the need for secondary processing steps, making the process more efficient and cost-effective. This topic is being actively researched and several recent studies have reported promising results, indicating the potential for SiC composites with in-situ formation of BN and Si_3N_4 to be used in high-temperature applications. Overall, this topic holds great potential for developing advanced ceramics with improved properties and wider application ranges. The purpose of the current investigation is to examine the effect of Si and B_2O_3 nitridation in the SiC composite aided with Al_2O_3. Also, the consequences of the formation of Si_3N_4 and BN in SiC composite on microstructural and physio-mechanical properties have been discussed.

2 Experimental Details

2.1 Materials

Commercially available raw materials that were utilized and their information attributed to purity, particle size, and supplier are exhibited in Table 1. The Grading method was used in SiC to increase densification and reduce the overall porosity [27]. This grading was done using 30% 80/180 SiC, 30% 220F SiC and 40% 1 µm SiC. These materials were used for different ceramic composites according to the composition indicated in Table 2.

Table 1 Precursorsused details

Name	Purity	Particle size (µm)	Supplier
SiC 80/180	> 97.5%	50–70	Sigma Aldrich
SiC 220F	> 98%	40–45	Loba chemie
Ultrafine SiC	> 99%	< 1	CDH
Al_2O_3	> 98%	< 2	Sigma Aldrich
Si Metal	> 99.998%	< 45	Sigma Aldrich
B_2O_3	> 99.98%	< 1	Sigma Aldrich

2.2 Ball Milling

The above-mentioned raw materials in Table 1 were accurately weighted using a precise digital scale and then were dry mixed in different volume fractions in a ball mill for 4 h. During milling, a small amount of ethanol, 3% by weight, was added to the ball mill to prevent contamination and agglomeration of the powders. The ball milling had a ball-to-powder ratio of 1:10, with a cyclic interval of 15 min milling and then 15 min halt to prevent overheating and possible oxidation.

2.3 Cold Isostatic Pressing

The milled powders were mixed for 5 min in an agate mortar pestle with a few sprinkled droplets of binder (Dextrine). This was then isostatically pressed through a die in a bar with a dimension of $40 \times 10 \times 10$ mm, with a pressure of 200 MPa. This green compact was dried in a vacuum oven overnight and then sintered.

2.4 Sintering

For proper nitridation, the whole sintering of the prepared sample was carried under N_2 pressure of 0.1 MPa. The heating schedule for the samples is at 5 °C/min till it reaches 1000 °C, and post that 3 °C/min till 1450 °C. After holding the samples at 1450 °C for 1 h, they were gradually cooled. The heating rate, cooling rate, and cooling medium can affect densification and result in unwanted phases. The temperature was optimized for the formation of α-Si_3N_4 since at higher temperatures, α to β phase transformation of Si_3N_4 occurs more rapidly [28]. The prepared sintered composite samples are depicted in Fig. 1.

Table 2 Proportions of the specimens

Sample code	Graded SiC (Vol.%)	Al_2O_3 (Vol.%)	Si (Vol.%)	B_2O_3 (Vol.%)
SN1	80	15	5	-
SN2	75	15	10	-
SN3	70	15	15	-
SN4	65	15	20	-
SNB1	75	15	10	0
SNB2	70	15	10	5
SNB3	65	15	10	10
SNB4	60	15	10	15

A simplified chemical reaction that occurs between the precursors is shown in Eq. (1). Formation of Si_3N_4 and its α to β phase transformation are denoted in Eqs. (2) and (3). Due to low melting point, B_2O_3 liquidities first and upon reacting with Silicon nitride forms boron nitride and silicon dioxide. This can be seen in Eqs. (4), (5), and (6).

$$SiC + Si + Al_2O_3 + B_2O_3 \xrightarrow{Nitridation} SiC/Al_2O_3/Si_3N_4/BN \quad (1)$$

$$3Si(s) + 2N_2(s) \rightarrow \alpha - Si_3N_4(\mathrm{s}) \quad (2)$$

$$\alpha - Si_3N_4(s) \rightarrow \beta - Si_3N_4(s) \quad (3)$$

$$B_2O_3(\mathrm{s}) = B_2O_3(l) \quad (4)$$

$$B_2O_3(l) + Si_3N_4(s) \rightarrow 4BN(s) + 3SiO_2(\mathrm{s}) \quad (5)$$

$$SiO_2(l) + SiC(s) \rightarrow 2SiO(g) \uparrow + C\ (\mathrm{s}) \quad (6)$$

2.5 Phase Evolution

The phases present in the prepared composite were determined by X-Ray Diffraction (Rigaku Miniflex 600 Desktop XRD System) equipped with Ni filtered Cu kα (λ = 1.5417 A°) using 2° per minute scan rate, 0.02° step size within 2θ of 5° to 90° range. Further, to evaluate the phases present, Rietveld refinement was carried out using the Full-Prof program suite in Match! Software.

Fourier transform infrared (FTIR) spectroscopy was obtained with Thermo electron Scientific instruments LLC (Nicolet iS5) equipment to examine the nature and presence of different functional groups in the wavelength range of 4000–400 cm^{-1}.

Fig. 1 Sintered samples

2.6 Microstructural analysis

The morphology and microstructure examination of the samples was carried out using a High-Resolution Scanning Electron microscope (HR-SEM, Nova Nano SEM 450, FEI USA). To gain insight into the elemental composition, EDX was conducted using energy-dispersive X-ray spectroscopy (Team Pegasus integrated EDS-EBSD with octane plus and Hikari pro). The hardness indent SEM analysis was done using EVO SEM MA15/18 (Carl Zeiss microscopy ltd.). For all the SEM analysis, the sintered samples were first fine polished and then ultrasonicated in ethanol, followed by thermal etching in an oven at 100 °C overnight. The samples were then gold coated using Au sputtering for 120 s.

2.7 Physio-mechanical Characterization

2.7.1 Apparent Porosity and Bulk Density

The sample's apparent porosity and bulk density were determined using the Archimedes principle as per the international standard ISO 5017. At first, the dry weight of the prepared samples was measured, following which the sample was suspended in water, and then the soaked weight of the samples was measured. The mathematical calculation for apparent porosity and bulk density were determined using Eqs. (7) and (8), respectively.

$$\text{Apparent porosity (A.P.\%)} = \frac{m_2 - m_2}{m_{2-m_3}} \times 100 \quad (7)$$

$$\text{Bulk density (gm/cm}^3) = \frac{m_1}{m_2 - m_3} \quad (8)$$

Where m_1 = dry weight in gram (gm), m_2 = suspended weight (gm), and m_3 = soaked weight (gm).

2.7.2 Hardness and Flexural Strength

The hardness of the prepared composite samples was measured by the indentation method. The Vickers hardness tester (Bareiss Digi-test, VTP-6046) has been used at a load and dwell time of 10 kgf and 10 s, respectively. The flexural strength of composite samples was determined using a three-point bend test in an Electromechanical universal testing machine (HIECO HL 591) with a capacity of 10 kN.

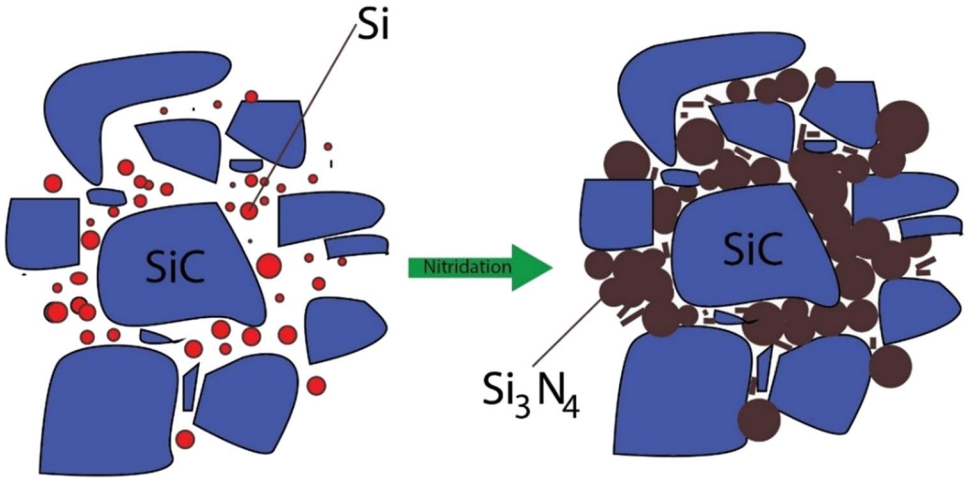

Fig. 2 Schematic of the densification mechanism due to Si_3N_4 formation

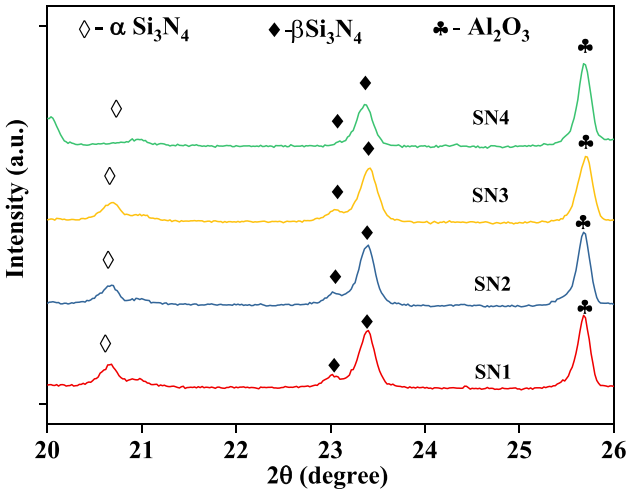

Fig. 3 X-ray diffraction patterns for sintered SN1, SN2, SN3, and SN4 composite samples

3 Result and Discussions

3.1 Effect of Si_3N_4 on SiC Composite

To examine the influence of Si_3N_4 on the SiC composite, varying percentages of Si were introduced in the samples denoted as SN1, SN2, SN3, and SN4, indicated with compositions in Table 2. The conversion and grain growth mechanism occurring during the nitridation densifies the overall composite (Depicted in Fig. 2). The brown spherical and rod-like structure denotes α and β phases of Si_3N_4, respectively.

In the present sintering condition, both α and β phases of Si_3N_4 can be formed due to increased α to β phase transformation of Si_3N_4 at a temperature above 1400 °C. XRD of the sintered samples SN1 to SN4, shown in Fig. 3, was confined to a range of 20° to 26° so that the changes in peak intensity of both α and β-Si_3N_4 could be visually distinguished. Further, Based on the intensity ratios of the reflection peaks of (101) and (210) in the β phase and (102) and (210) in the α phase, the relative quantities of α and β-phase were measured and estimated using the Gazzara and Messier method [19, 29].

Table 3 Weight percentage of α and β Si_3N_4

Sample code	β - Si_3N_4 (wt.%)	α-Si_3N_4 (wt.%)
SN1	54.75	45.25
SN2	59.65	40.35
SN3	64.92	35.08
SN4	72.85	27.15

$$\beta - Si_3N_4(wt\%) = \frac{I_{\beta(101)} + I_{\beta(210)}}{[I_{\alpha(102)} + I_{\alpha(201)} + I_{\beta(101)} + I_{\beta(210)}]} \quad (9)$$

The obtained results of the samples are listed in Table 3. As the percentage of Si increased the α phase content of the samples appeared to be in decreasing order, which is due to the rapid phase formation of β-Si_3N_4 at scattered locations. This β-Si_3N_4 acts like a seed for more β-Si_3N_4 formation while suppressing the formation of α-Si_3N_4. The peak intensity of α-Si_3N_4 is also clearly seen in XRD Fig. 3 to be decreasing as Si content increases.

3.1.1 Microstructural Analyses

The addition of Si_3N_4 can affect the microstructural and mechanical properties of prepared composite samples. The SEM images of sintered SN1, SN2, SN3 and SN4 composite samples are represented in Fig. 4. All samples illustrate good densification with tiny whitish particles denoting the

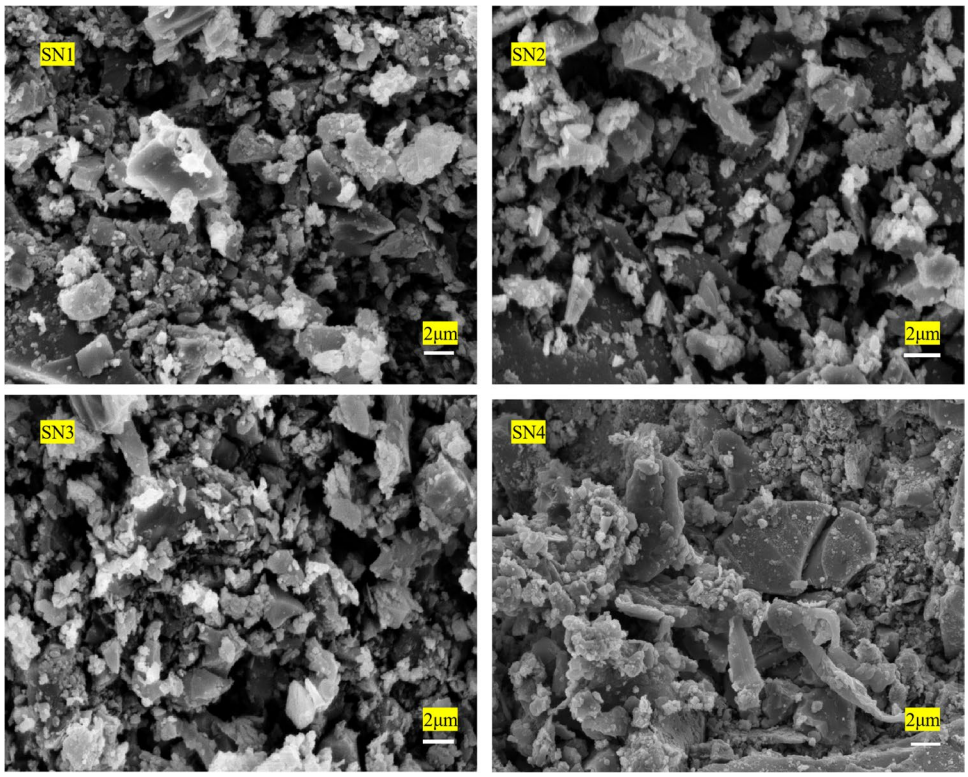

Fig. 4 SEM micrographs for sintered SN1, SN2, SN3 and SN4 composite samples

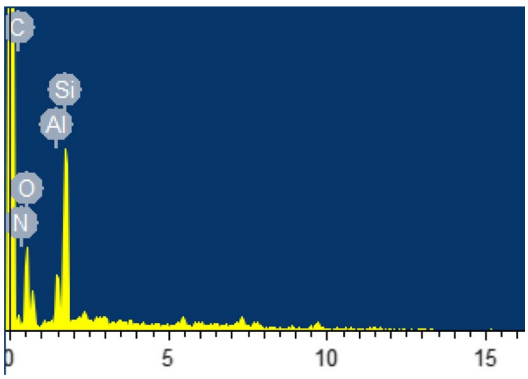

Elements	Wt. %
C	20.6
O	8.2
N	6.9
Al	9.7
Si	54.6

Fig. 5 EDX of sample SN2 along with its atomic content %

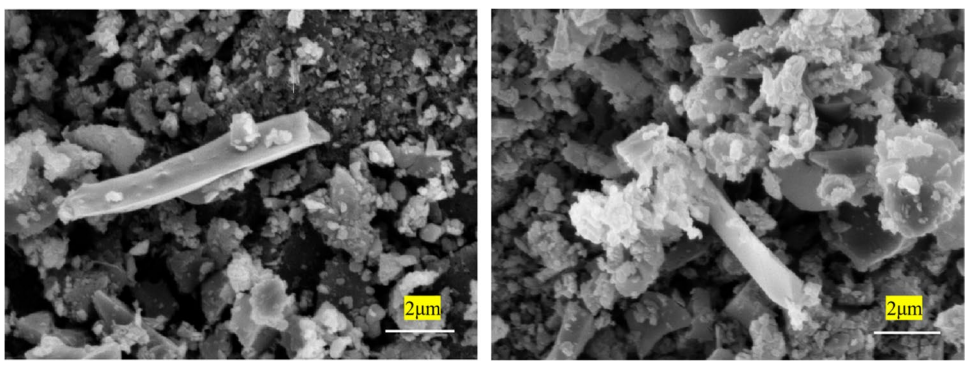

Fig. 6 SEM of elongated grains of β-Si_3N_4 particles

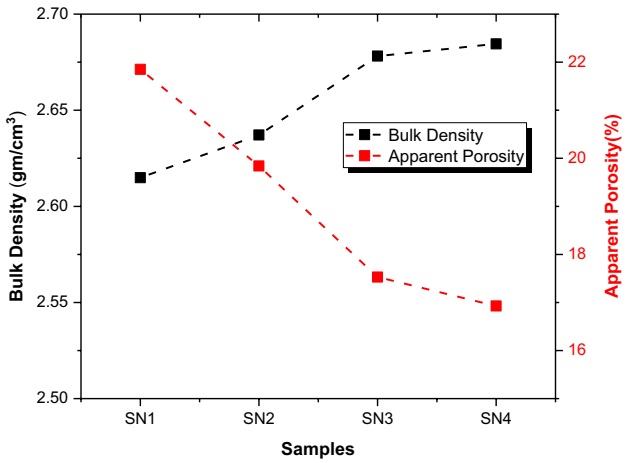

Fig. 7 Bulk Density and apparent porosity of Sintered SN coded Samples

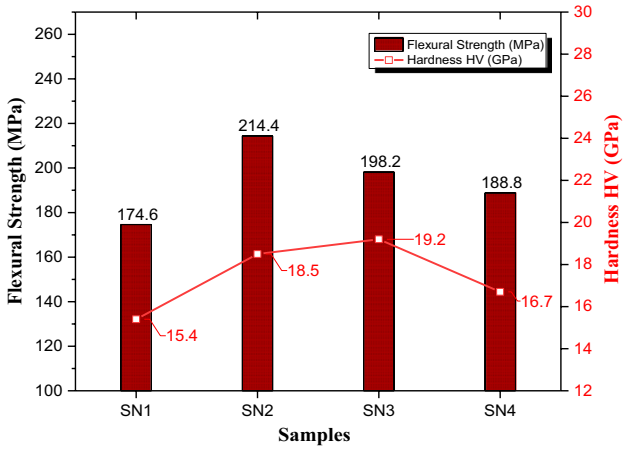

Fig. 8 Flexural strength and hardness results of SN samples

Al_2O_3 content in the composite matrix. SiC can also be seen in various shapes and sizes, resulting from different grades of SiC. The samples SN1 to SN4 show an increasing order of rod-like structure, which represents β-Si_3N_4 structure. Also, it can be seen that the size of this rod structure is also increasing, which is due to the seeding behavior of β phase (Fig. 5). The energy dispersive x-ray (EDX) analysis confirms the constituent elements in the composite system and supports the XRD analyses result. Figure 6 shows SEM image of the nucleation and growth process of elongated rod-shaped β-Si_3N_4. Once β-Si_3N_4 is formed, it encourages the α to β-Si_3N_4 transformation while behaving like a seed triggering grain growth to form micrometer-sized grain.

3.2 Physio-mechanical Characterization

The sample's bulk density and apparent porosity were measured, and Fig. 7 represents the data with varying Si content i.e., SN1 to SN4. The bulk density slightly increased from 2.6149 to 2.6845 gm/cm^3 owing to the increase in Si_3N_4 formation. The apparent porosity also reduces from 21.85 to 16.92% due to the Si_3N_4 filling voids mechanism, as illustrated in Fig. 2.

Figure 8 depicts the hardness and flexural strength of the sintered SN composite series. The composite SN2 with 10% Si has the highest flexural strength of 214.4 MPa, while SN3 with 15% Si shows the highest hardness of 19.2 GPa. Microstructural properties such as phases, grain size, and porosity should be the main contributors in increasing the hardness and flexural strength. The later decline result from increased β - Si_3N_4 formation and its elongated grain.

3.3 Samples Empowered with BN and Si_3N_4

3.3.1 Phase Evolution

The X-ray diffraction patterns (XRD) for sintered SNB1, SNB2, SNB3, and SNB4 powder samples are shown in Fig. 9a. The XRD spectra were analyzed using X-pert high score software, and peaks were indexed with standard JCPDS reference. The XRD analyses revealed that the peaks of SiC (96-231-1059), α-Si_3N_4(96-100-1240), β - Si_3N_4 (96-100-1250), boron nitride (96-201-6174) and Al_2O_3 (96-100-0060) which were matched adequately with respective JCPDS reference without any dissociation. BN has low crystal degree and thus show weak peaks in XRD [26]. Rietveld refinement reveals the relative phases and elemental content of composite SNB3, depicted in Fig. 9b and c.

3.3.2 Fourier transform infrared spectroscopy (FTIR) analyses

The presence of functional groups and structural bonds in the prepared composite system was investigated using FTIR spectra. Figure 10 represents the FTIR spectra of the SNB3 composite. The characteristic peaks observed at ~ 401, 437, 460, 503, 570, and 650 cm^{-1} correspond to alumina [30]. The peaks near 570 and 670 cm^{-1} represent the stretching vibration of AlO_6 octahedra [31]. The intensity of these peaks increases with the increase in the composition of Al_2O_3. The Si–Si stretching mode was observed at 685 cm^{-1}. The bands observed at 785 and 830 cm^{-1} correspond to Si–C [32]. The symmetric and asymmetric stretching of Si–N was observed at 480 and 840 cm^{-1} [33]. The symmetric Si–N stretching has three Si atoms bonded

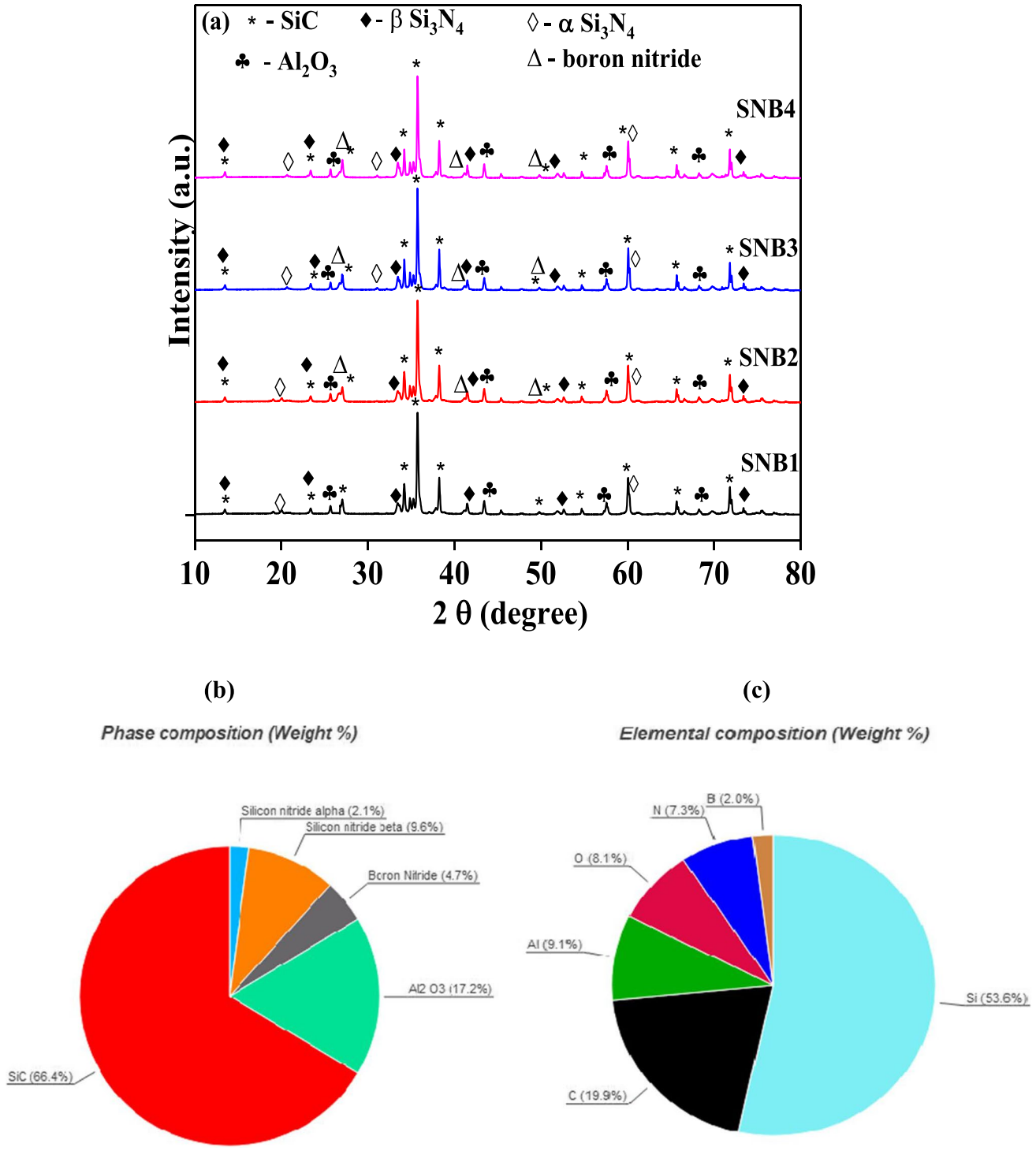

Fig. 9 **a** X-ray diffraction patterns for sintered SNB1, SNB2, SNB3, and SNB4 composite samples, **b** weight % of phases, and **c** elemental composition in the composite obtained from Rietveld refinement.

with the N atom, also known as Si breathing mode [34]. The longitudinal optical and transverse optical vibrations of boron nitride (BN) resonate at ~ 1067 and 1370 cm^{-1} [35]. The results indicate that during sintering, nitridation of Si and B_2O_3 occurs transforming into silicon nitride and boron nitride with no further reaction post sintering. The FTIR results corroborate the XRD and the reaction stated in Eqs. (1) to (6).

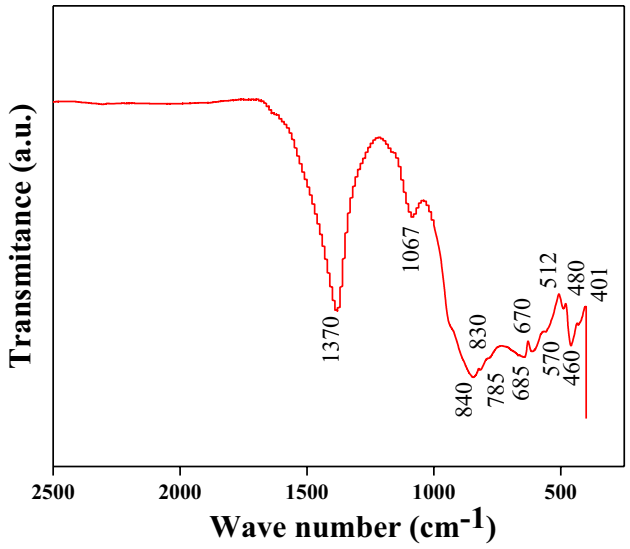

Fig. 10 Fourier transform infrared (FTIR) spectra of sintered SNB3 composite sample

3.3.3 Microstructural analyses

Figure 11 shows the SEM micrographs of sintered SNB1, SNB2, SNB3, and SNB4 composite samples. SEM images demonstrate good densification, which confirms proper sintering. A spherical shape α-Si_3N_4 is seen surrounding the SiC. The rod-like structure representing β-Si_3N_4 is randomly distributed with long elongated grain growth. The energy dispersive x-ray (EDX) analyses confirm the constituent elements in the composite system, which is in range with the Rietveld refinement results. EDX can only detect elements with atomic numbers higher than boron, so EDX results have the remaining constituents apart from Boron (Fig. 12).

3.4 Physio-mechanical Characterization of SNB Samples

The physio-mechanical properties, such as bulk density, apparent porosity, hardness, and flexural strength of the SNB samples, were measured post sintering. Figures 13 and 14 represent this data with varying B_2O_3 content. The bulk density of SNB1 with 0 wt.% B_2O_3 is 2.632 gm/cm^3 while the porosity is 19.698%, which is similar to SN2 composite. The initial decrease in porosity can be due to void filling, while the later increases are majorly due to exit gases like SiO. A higher B_2O_3 amount would account for more reaction with Si_3N_4 to form SiO gases, as indicated in Eq. 5. These exit gases are core factors for increasing the pore size, which increases the porosity. Boron Nitride, known for its hardness, consistently improves the hardness of the composite while positively impacting flexural strength. The decrease in flexural strength in SNB4 samples can be due to an increase in SiO gas formation, resulting in more micro pores allowing crack propagation.

The Vickers indentation on sintered SNB1, SNB2, SNB3, and SNB4 composite samples is shown in Fig. 15. It is observed that the depth of indent in samples; SNB1 has maximum and SNB4 demonstrate minimum indent depth.

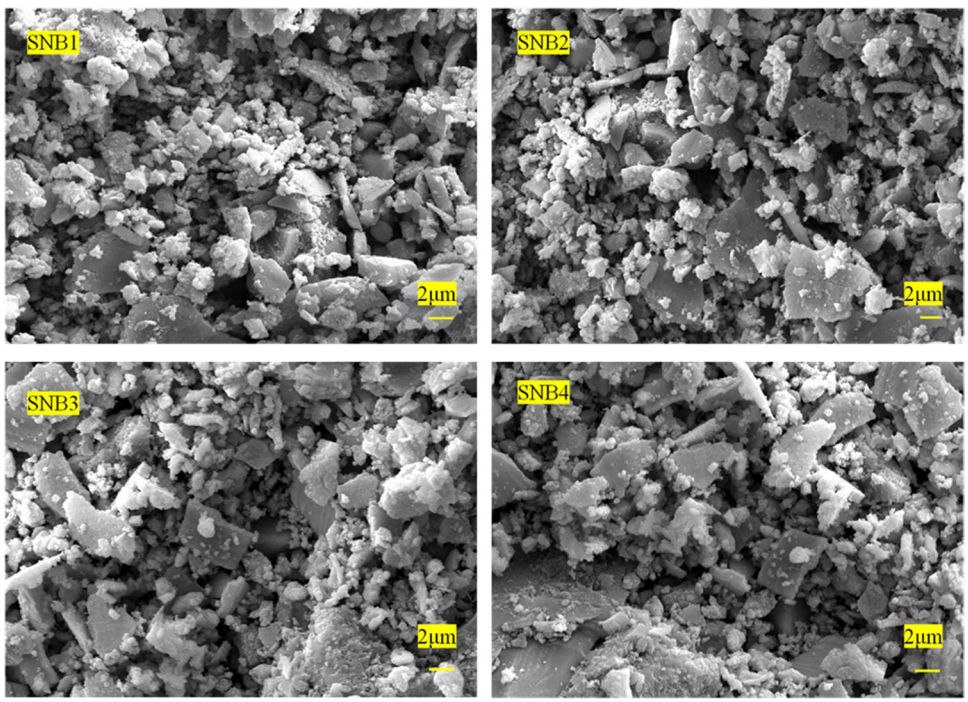

Fig. 11 SEM micrographs for sintered SNB1, SNB2, SNB3, and SNB4 composite samples

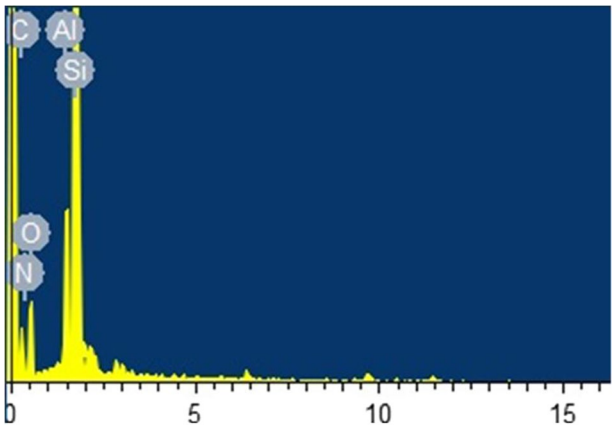

Elements	Wt. %
C	19.8
O	6.9
N	7.9
Al	10.5
Si	54.9

Fig. 12 EDX of sample SNB3 along with its atomic content %

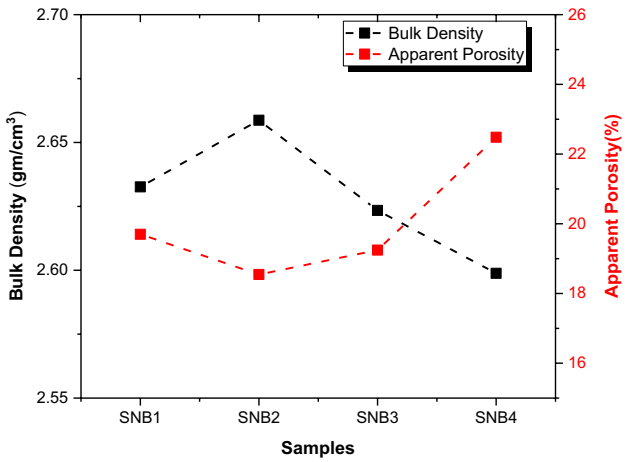

Fig. 13 Bulk Density and apparent porosity graphs of Sintered SNB coded Samples

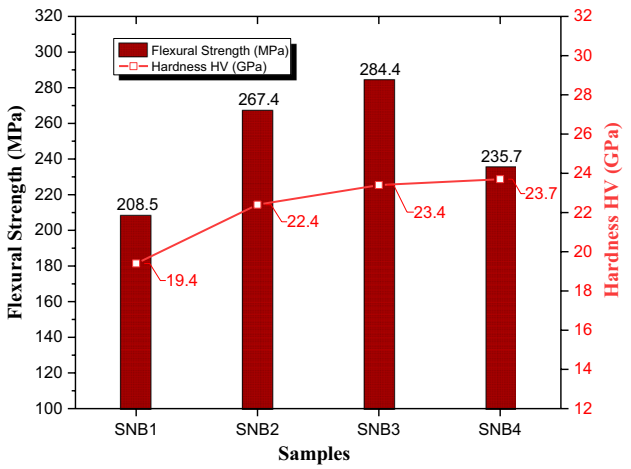

Fig. 14 Flexural strength and hardness results of SNB samples

The hardness of composite samples increases as the content of boron nitride (from 19.4 to 23.7 GPa). The SEM images also reveal good densification and the brittle nature of prepared sample.

4 Conclusion

A method was proposed to prepare the insitu formation of BN and Si_3N_4 on SiC-based composite with Al_2O_3 as a sintering additive. The following conclusions were drawn:

(1) Insitu formation of Si_3N_4 and BN with nitridation of Si and B_2O_3 was successfully achieved and can be used as a cost-effective alternative with improved thermo-mechanical properties. It is also processed at a much lower temperature, providing a more viable and environment-friendly fabrication.

(2) A denser Si_3N_4-SiC composite was fabricated compared to other reported reaction-bonded composites, with flexural strength reaching up to 214 MPa and a hardness value of 19.2 GPa. The addition of 10 wt% Si showed this result while further increasing decreased the mechanical strength. It might be accounted for the elongated β-phase formation of Si_3N_4.

(3) SN2 and SNB1 are of identical composition sintered in different time frames, yielding nearly similar properties validating the process and its repeatability. It also suggests that the formation of α and β Si_3N_4 depends on the sintering condition and its composition. Thus, it can be tailored for a particular application with a required set of properties.

(4) Adding different weight % of B_2O_3 in 10% Si in composite samples (SNB) resulted in the homogenous formation of BN, which helps in improving the thermal and mechanical properties. Although at higher B_2O_3 concentration, the flexural strength of the composite decreases, it still retains overall hardness.

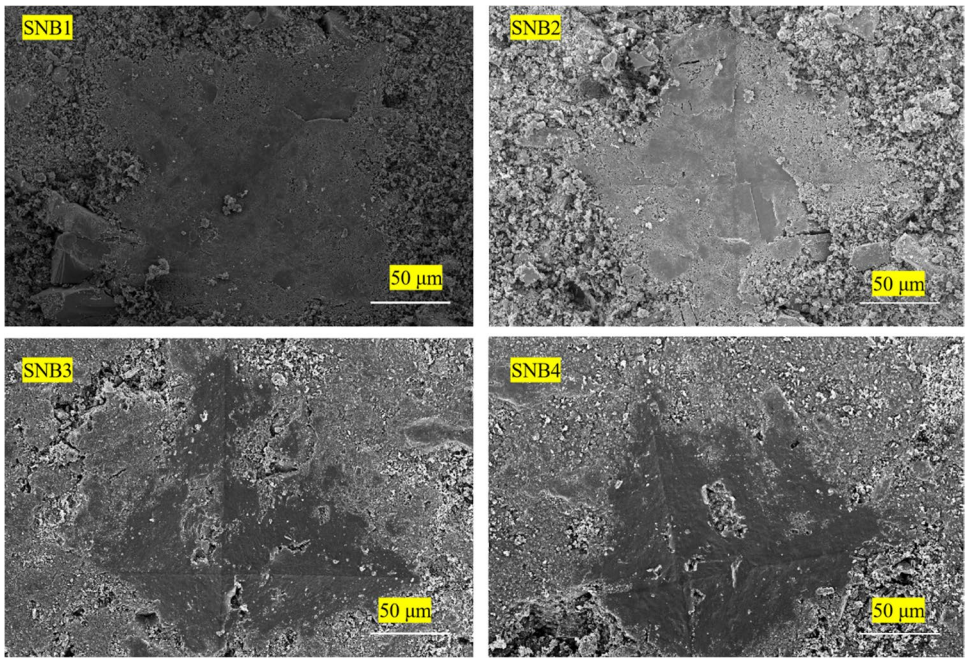

Fig. 15 SEM micrographs of Vickers indentation on sintered SNB1, SNB2, SNB3, and SNB4 composite samples at 10kgf load

(5) In an application where porous composite is required without severely degrading the mechanical properties this approach could be utilized by not allowing densification and promoting the formation of β Si_3N_4 and BN.

Acknowledgements The financial support by Science and Engineering Research Board (SERB) of Department of Science and Technology (DST), Government of India, is gratefully acknowledged. The authors also acknowledge the Central Instrument Facility, IIT (BHU), Varanasi, India, for the instrumentation facility and support.

Author Contributions Aman Singh designed the study, conducted the experiments, and wrote the manuscript. Jyoti Kumari and Nayan Kumar Debnath collected the data and contributed to the analysis. Prof Vinay Kumar Singh and Dr. R. K. Chaturvedi supervised the project. All authors reviewed and approved the final manuscript.

Data Availability All data generated or analyzed during this study will be made available on request.

Declarations

Research Involving Human Participants and Animals This article does not contain any studies with human or animal subjects.

Statement on the Welfare of Animals This article does not contain any studies with human participants or animals performed by any authors.

Ethics approval and consent to participate We comply to the ethical standards. We provide our consent to take part.

Consent for Publication All the authors are giving consent to publish.

Competing Interests The authors declare no competing interests.

References

1. Jana P, Oza MJ, Schell KG et al (2022) Study of the elastic properties and thermal shock behavior of Al–SiC-graphite hybrid composites fabricated by spark plasma sintering. Ceram Int 48:5386–5396. https://doi.org/10.1016/j.ceramint.2021.11.082
2. Kovalčíková A, Kurek P, Balko J et al (2014) Effect of the counterpart material on wear characteristics of silicon carbide ceramics. Int J Refract Met Hard Mater 44:12–18. https://doi.org/10.1016/j.ijrmhm.2014.01.006
3. Zhang W, Wang H, Jin Z (2005) Gel casting and properties of porous silicon carbide/silicon nitride composite ceramics. Mater Lett 59:250–256. https://doi.org/10.1016/J.MATLET.2004.07.059
4. Zhang J, Xiao G, Yi M et al (2022) High-temperature mechanical properties of ZrB2/SiC/Si3N4 ceramic tool materials with dual composite architectures. Ceram Int 48:1038–1046. https://doi.org/10.1016/J.CERAMINT.2021.09.189
5. Santhosh Kumar S, Devaiah M, SeshuBai V, Rajasekharan T (2012) Mechanical properties of SiC p/Al 2O 3 ceramic matrix composites prepared by directed oxidation of an aluminum alloy. Ceram Int 38:1139–1147. https://doi.org/10.1016/J.CERAMINT.2011.08.042
6. Wang H-f, Bi Y-b, Zhou N-s, Zhang H-j (2016) Preparation and strength of SiC refractories with in situ β-SiC whiskers as bonding phase. Ceram Int 42:727–733. https://doi.org/10.1016/J.CERAMINT.2015.08.172
7. Hnatko M, Galusek D, Šajgalík P (2004) Low-cost preparation of Si3N4-SiC micro/nano composites by in-situ carbothermal reduction of silica in silicon nitride matrix. J Eur Ceram Soc 24:189–195. https://doi.org/10.1016/S0955-2219(03)00604-6
8. Oguntuyi SD, Malatji N, Shongwe MB et al (2022) The influence of Si3N4 on the microstructure, mechanical properties and the wear performance of TiB2–SiC synthesized via spark plasma sintering. Int J Light Mater Manuf 5:326–338. https://doi.org/10.1016/J.IJLMM.2022.04.004

9. Suri J, Shaw LL (2014) Liquid phase sintering of Si3N4/SiC nanopowders derived from silica fume. Ceram Int 40:9179–9187. https://doi.org/10.1016/J.CERAMINT.2014.01.135
10. Greil P, Petzow G, Tanaka H (1987) Sintering and HIPping of silicon nitride-silicon carbide composite materials. Ceram Int 13:19–25. https://doi.org/10.1016/0272-8842(87)90034-4
11. Zhang Y, Yao D, Zuo K et al (2021) Effects of different types of sintering additives and post-heat treatment (PHT) on the mechanical properties of SHS-fabricated Si3N4 ceramics. Ceram Int 47:22461–22467. https://doi.org/10.1016/J.CERAMINT.2021.04.255
12. Shahrestani S, Ismail MC, Kakooei S, Beheshti M (2021) Microstructure, phase compositions and mechanical properties of slip cast sintered SiC/Si3N4 composites. Ceram Int 47:13173–13180. https://doi.org/10.1016/J.CERAMINT.2021.01.182
13. Kanno Y (1985) Properties of SiC, Si3N4 and SiO2 ceramic powders produced by vibration ball milling. Powder Technol 44:93–97. https://doi.org/10.1016/0032-5910(85)85027-0
14. Weimer AW, Bordia RK (1999) Processing and properties of nanophase SiC/Si3N4 composites. Compos Part B Eng 30:647–655. https://doi.org/10.1016/S1359-8368(99)00039-6
15. Sun L, Fang J, Guo S et al (2022) Effect of MgO/Al2O3 ratio on the crystallization behaviour of Li2O–MgO–Al2O3–SiO2 glass-ceramic and its wettability on Si3N4 ceramic. Ceram Int 48:20053–20061. https://doi.org/10.1016/J.CERAMINT.2022.03.281
16. Zhu TB, Li YW, Sang SB, Jin SL (2016) The influence of Al and Si additives on the microstructure and mechanical properties of low-carbon MgO-C refractories. J Ceram Sci Technol 7:127–134. https://doi.org/10.4416/JCST2015-00055
17. Ganesh I, Sundararajan G, Olhero SM et al (2010) A novel colloidal processing route to alumina ceramics. Ceram Int 36:1357–1364. https://doi.org/10.1016/J.CERAMINT.2010.01.022
18. Hu HL, Zeng YP, Zuo KH et al (2015) Synthesis of porous Si3N4/SiC ceramics with rapid nitridation of silicon. J Eur Ceram Soc 35:3781–3787. https://doi.org/10.1016/J.JEURCERAMSOC.2015.06.028
19. Kong JH, Ma HJ, Jung WK et al (2021) Self-reinforced and high-thermal conductivity silicon nitride by tailoring α-β phase ratio with pressureless multi-step sintering. Ceram Int 47:13057–13064. https://doi.org/10.1016/J.CERAMINT.2021.01.169
20. Chen J, Chen K, Liu YG et al (2014) Effect of Al2O3 addition on properties of non-sintered SiC–Si3N4 composite refractory materials. Int J Refract Met Hard Mater 46:6–11. https://doi.org/10.1016/J.IJRMHM.2014.05.001
21. Zhao J, Stearns LC, Harmer MP et al (1993) Mechanical behavior of alumina-silicon carbide "nanocomposites." J Am Ceram Soc 76:503–510. https://doi.org/10.1111/j.1151-2916.1993.tb03814.x
22. Hossain S, Mamunur Rahman MD, Chawla D et al (2020) Fabrication, microstructural and mechanical behavior of Al-Al2O3-SiC hybrid metal matrix composites. In: Materials today: proceedings. Elsevier Ltd, pp 1458–1461
23. Ju M, Cai M, Nie J et al (2021) Advanced Al2O3–SiC–SiO2–C refractories with B2O3 addition. Ceram Int 47:29525–29531. https://doi.org/10.1016/j.ceramint.2021.06.243
24. Noviyanto A, Yoon DH, Lee K et al (2013) Effect of hexagonal-BN on phase transformation of additive-free Si3N4/SiC nanocomposites prepared from amorphous precursor. Trans Nonferrous Met Soc China 23:420–425. https://doi.org/10.1016/S1003-6326(13)62479-6
25. Li X, Zhang L, Yin X, Yu Z (2010) Mechanical and dielectric properties of porous Si3N4–SiC(BN) ceramic. J Alloys Compd 490:L40–L43. https://doi.org/10.1016/J.JALLCOM.2009.10.107
26. Yu Y, Luo R, Xiang Q et al (2015) Anti-oxidation properties of a BN/SiC/Si3N4–ZrO2–SiO2 multilayer coating for carbon/carbon composites. Surf Coatings Technol 277:7–14. https://doi.org/10.1016/J.SURFCOAT.2015.06.072
27. Chen J, Li N, Wei Y et al (2017) Synthesis of Si3N4/SiC reaction-bonded SiC refractories: the effects of Si/C molar ratio on microstructure and properties. Ceram Int 43:16518–16524. https://doi.org/10.1016/J.CERAMINT.2017.09.036
28. Bučevac D, Boškovic S, Matović B (2008) Kinetics of the α-β phase transformation in seeded Si 3N4 ceramics. Sci Sinter 40:263–270. https://doi.org/10.2298/SOS0803263B
29. Gazzara CP, Messier DR (1977) Determination of phase content of Si3N4 by X-ray diffraction analysis. J Am Ceram Soc 56:777–780
30. Vasconcelos DCL, Nunes EHM, Vasconcelos WL (2012) AES and FTIR characterization of sol–gel alumina films. J Non Cryst Solids 358:1374–1379. https://doi.org/10.1016/J.JNONCRYSOL.2012.03.017
31. Padmaja P, Anilkumar GM, Mukundan P et al (2001) Characterisation of stoichiometric sol–gel mullite by fourier transform infrared spectroscopy. Int J Inorg Mater 3:693–698. https://doi.org/10.1016/S1466-6049(01)00189-1
32. Mohapatra S, Sakthivel R, Roy GS et al (2011) Synthesis of β-SiC powder from bamboo leaf in a DC extended thermal plasma reactor. Mater Manuf Process 26:1362–1368. https://doi.org/10.1080/10426914.2011.557127
33. Tsu DV, Lucovsky G, Mantini MJ (1986) Local atomic structure in thin films of silicon nitride and silicon diimide produced by remote plasma-enhanced chemical-vapor deposition. Phys Rev B 33:7069. https://doi.org/10.1103/PhysRevB.33.7069
34. Wang YQ, Wang YG, Cao L, Cao ZX (2003) High-efficiency visible photoluminescence from amorphous silicon nanoparticles embedded in silicon nitride. Appl Phys Lett. https://doi.org/10.1063/1.1621462
35. Shin H, Guan J, Zgierski MZ et al (2015) Covalent functionalization of boron nitride nanotubes via reduction chemistry. ACS Nano 9:12573–12582. https://doi.org/10.1021/ACSNANO.5B06523/ASSET/IMAGES/LARGE/NN-2015-065234_0008.JPEG